High spin spectroscopy and shape coexistence in ^{73}As

M. Kumar Raju,[1,2,*] P. V. Madhusudhana Rao,[1] S. K. Tandel,[3] P. Sugathan,[1,4] R. P. Singh,[4] S. Muralithar,[4] T. Seshi Reddy,[1] B. V. Thirumala Rao,[1] Jie Meng,[5] Shuangquan Zhang,[5] Jian Li,[5] Q. B. Chen,[5] Bin Qi,[6] and R. K. Bhowmik[4]

[1]*Nuclear Physics Department, Andhra University, Visakhapatnam 530003, India*

[2]*Department of Physics, University of the Western Cape, P/B X17, Bellville ZA-7535, South Africa*

[3]*UM-DAE Centre for Excellence in Basic Sciences, Mumbai 400098, India*

[4]*Inter-University Accelerator Centre, Aruna Asaf Ali Marg, New Delhi 110067, India*

[5]*School of Physics, State Key Laboratory of Nuclear Physics and Technology, Peking University, Beijing 100871, China*

[6]*School of Space Science and Physics, Shandong University at Weihai, 264209 Weihai, China*

(Received 29 September 2015; published 29 December 2015)

High spin states in ^{73}As have been investigated through the fusion-evaporation reaction ^{64}Ni(^{12}C, $p2n$)^{73}As with an incident beam energy of 55 MeV. The level scheme has been extended up to $J^{\pi} = (37/2^{-})$ and excitation energy ~8.7 MeV with the addition of 30 new γ-ray transitions. The microscopic origins of the observed positive- and negative-parity band structures are discussed in the context of the particle rotor model. Nucleon alignments and shape evolution with increasing angular momentum are discussed in the framework of the cranked shell model and relativistic mean-field calculations. The results offer insight into the nature of the observed band structures and indicate prolate-oblate shape coexistence between positive- and negative-parity bands at low spin.

DOI: 10.1103/PhysRevC.92.064324 PACS number(s): 23.20.Lv, 21.10.Re, 21.60.Cs, 27.50.+e

I. INTRODUCTION

Nuclei in the mass $A \sim 70$ region exhibit complex behavior with increasing angular momentum. Shape coexistence and a rapid transition between prolate and oblate deformations as a function of both proton and neutron number as well as spin and excitation energy are observed in this region. These features are attributed to the dynamical interplay between single-particle and collective degrees of freedom and due to the presence of deformed shell gaps at $N = Z = 34$, 36, and 38. These shell gaps favor competing oblate and prolate structures, which coexist over a small range of spin, a phenomenon referred to as shape coexistence. The coexistence of different nuclear shapes has been observed in several even-even nuclei in this region, e.g., $^{72-74}$Se [1–3] and $^{74-78}$Kr [4–6], but limited information exists thus far for odd-A and odd-odd nuclei. Positive-parity decoupled rotational bands have been identified in the odd-A As and Br [7–10] isotopes. The decoupled nature of these bands is interpreted to arise from configurations involving particles in the $g_{9/2}$ proton subshell, which decouples from the core due to the strong Coriolis force. Since the structure of these bands depend on the core deformation (oblate or prolate), the spectroscopic study of the decoupled configurations built on the deformation-driving $g_{9/2}$ orbital offers a unique experimental opportunity for investigating shape evolution in this mass region.

Odd-A arsenic isotopes $^{67-73}$As [11–14] have been studied up to $J^{\pi} = 33/2^{+}$,$53/2^{+}$,$37/2^{-}$, and $25/2^{+}$, respectively. Although the observed band structures of ^{67,69,71}As [11–13] have certain common features, with increasing neutron number, differences in structure are evident. For example, a systematic comparison of positive-parity bands based on the $\pi g_{9/2}$ configuration in these isotopes reveals that the energy of the $13/2^{+} \rightarrow 9/2^{+}$ transition decreases from 943 keV in ^{67}As [11] to 609 keV in ^{73}As [14]. This is indicative of the gradual increase in collectivity with neutron number. These nuclei are predicted to have rapid shape transitions with increasing angular momentum due to the occupation of the deformation-driving $g_{9/2}$ orbital by valence nucleons and also due to large deformed shell gaps in the Nilsson diagram. For example, total Routhian surface (TRS) calculations predict that the nuclear shape changes from oblate in ^{65}As to prolate in ^{69}As, and to a γ-soft shape in ^{71}As at low spin. Thus, the triaxial deformation parameter (γ) varies across these isotopes, and it is therefore interesting to explore ^{73}As.

The low spin structure of odd-A ^{73}As has been reported earlier employing γ-spectroscopic methods with the (p,$n\gamma$) reaction [15,16]. Later, the positive-parity, yrast band above the 428.2-keV $9/2^{+}$ isomeric state was reported up to $J^{\pi} = 25/2^{+}$, and excitation energy ~4.1 MeV in studies using heavy-ion reactions: ^{58}Fe(^{18}O, $p2n$)^{73}As and ^{71}Ga(α, $2n$)^{73}As [14]. The origin of low spin states was interpreted by several authors using various theoretical models [14,15,17–19], such as the particle-plus-rotor model and Coriolis coupling model. In this work, we have presented high spin information in both positive- and negative-parity bands, along with non-yrast band structures. The deduced band structures and shape change have been analyzed using the cranked shell model (CSM) and particle rotor model (PRM) approaches.

The present article is organized as follows. In Sec. II, experimental details and the level scheme of ^{73}As are discussed. Section III includes a discussion on the level structures based on the cranked shell model (CSM) calculations and the shape evolution in ^{73}As in the context of relativistic mean-field (RMF) calculations. Further, the observed band structures are compared with the triaxial PRM calculations in Sec. III C. A brief summary is presented in Sec. IV.

II. EXPERIMENTAL DETAILS AND RESULTS

High spin states in ^{73}As were populated using the fusion-evaporation reaction ^{64}Ni(^{12}C, $p2n$)^{73}As with an incident

*kumar8284@gmail.com

beam energy of 55 MeV. The ^{12}C beam, with ∼1 pnA current, was delivered by the 15UD Pelletron accelerator [20] at Inter-University Accelerator Centre (IUAC), New Delhi, India. The target used in this experiment was isotopically enriched ^{64}Ni with thickness ∼1.5 mg/cm^2 on a thick (∼7 mg/cm^2) Au backing. The γ rays deexciting residual nuclei were detected with the Gamma Detector Array (GDA) [21,22]. This facility comprised of 12 Compton suppressed n-type hyperpure germanium (HPGe) detectors. These detectors were arranged in three groups, each consisting of four detectors. These were mounted coaxially in anti-Compton shields subtending angles 50°, 98°, 144° with respect to the beam direction. The distance between the target and HPGe detectors was ∼18 cm. The energy calibration and relative photopeak efficiency of the GDA array were obtained using ^{152}Eu and ^{133}Ba standard radioactive sources.

A total of about 13×10^7 twofold or higher γ-γ coincidences were recorded in event-by-event mode using an online CAMAC-based data acquisition system called Freedom [23,24]. The trigger condition was set such that data were collected when at least two detectors fired in coincidence. About 20% of the recorded events correspond to the nucleus of interest ^{73}As. The offline data analysis was carried out using programs CANDLE, INGASORT [25], and RADWARE [26]. The recorded γ-γ coincidence data were sorted into a two-dimensional $4k \times 4k$ symmetric E_γ-E_γ matrix with energy dispersion 0.5 keV/channel using the sorting routine INGASORT [25]. This was the primary data set used for the construction of the level scheme. One-dimensional energy spectra were extracted from these matrices by setting gates on specific γ energies.

The multipolarity of the γ transitions was assigned using the directional correlation orientation (DCO) ratio technique [27]. For this purpose, angle-dependent matrices were constructed by including energies of γ rays from all detectors at forward or backward angles on one axis and the coincidence γ energies from the detectors at 98° on the other axis. The experimental DCO ratio for the present work is defined as the intensity (I) of a measured transition at 50° or 144° when gated on a reference γ ray at 98°, divided by the intensity of a measured transition at 98° when gated on a reference γ ray at 50° or 144° (where the reference γ ray is of known multipolarity). The expression for the DCO ratio is

$$R_{\mathrm{DCO}} = \frac{I_{\gamma_1} \text{ at } 50^\circ/144^\circ \text{ gated by } \gamma_2 \text{ at } 98^\circ}{I_{\gamma_1} \text{ at } 98^\circ \text{ gated by } \gamma_2 \text{ at } 50^\circ/144^\circ}. \quad (1)$$

If the gating transition is of stretched quadrupole multipolarity then this ratio is ∼1 for pure quadrupole transitions and ∼0.5 for pure dipole ones. If the gating transition is of dipole multipolarity than the ratio is between 0–2 depending on the mixing ratio, and is 1 for pure dipoles.

Level scheme of ^{73}As

In the present work, the level scheme of ^{73}As has been extended to $J^\pi = (37/2^-)$ and excitation energy ∼8.7 MeV. The partial level scheme of ^{73}As obtained from the present work is shown in Fig. 1. The γ-ray and level energies are rounded off to the nearest integer. The level scheme is arranged into three main bands, labeled band B1, B2, and B3 for reference in the text. The observed low-spin structure in the present work is consistent with the reported levels in Ref. [14]. The yrast positive-parity band B1 and negative-parity bands B2 and B3 have been extended to $J^\pi = (37/2^+)$, $(37/2^-)$, and $(27/2^-)$, respectively. A total of 30 new γ-ray transitions belonging to ^{73}As have been identified and placed in the level

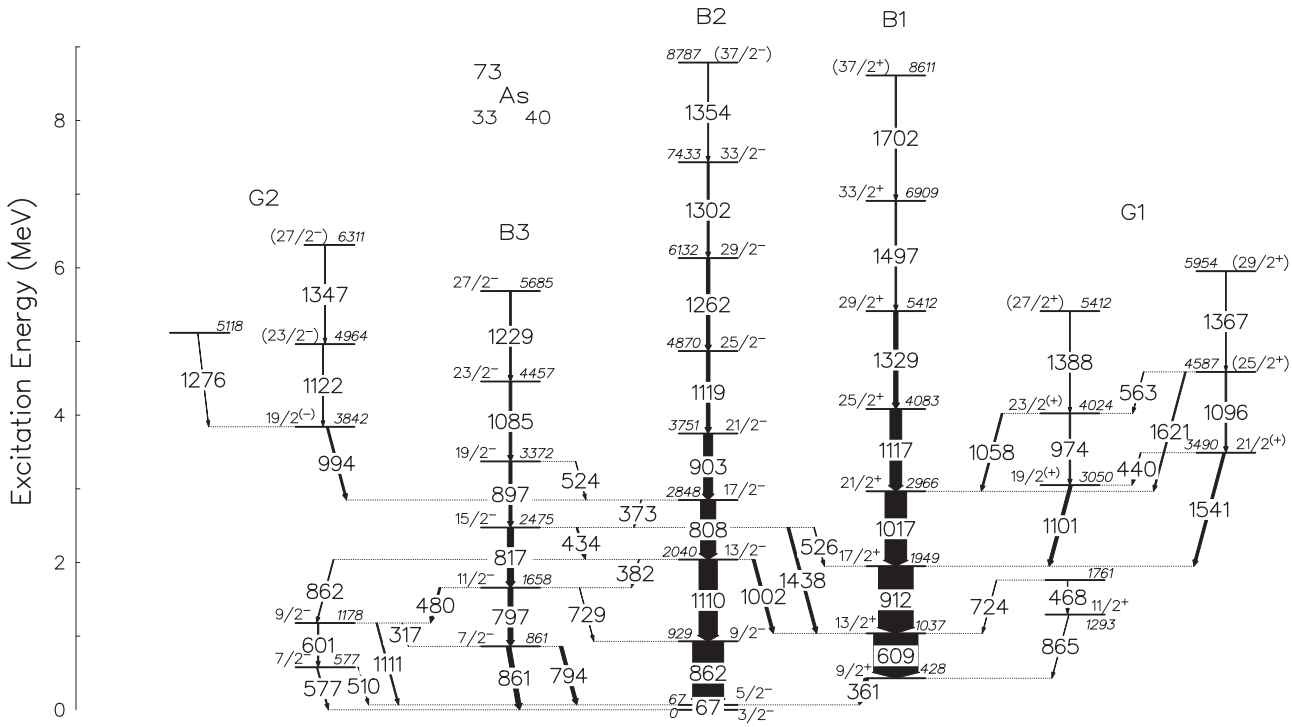

FIG. 1. Partial level scheme of ^{73}As obtained from the present work. Bands are labeled as B1, B2, B3, G1, and G2 for reference in the text.

scheme based on γ-γ coincidence relationships and intensity arguments. The relative intensities of γ rays are determined from the gated spectra obtained from the E_γ-E_γ symmetric matrix. The intensity values are normalized with respect to the 609-keV γ-ray transition. The spins and parities for known low-lying states were adopted from the previous work [14], and these values are used as a reference for multipolarity assignments to the new transitions. The DCO ratios are obtained from the angle-dependent matrices by using gates on known quadrupole transitions as a reference. The γ-ray energies, measured relative intensities, directional correlation orientation (DCO) ratios, multipolarities of observed γ rays and spin-parity assignments for the levels in ^{73}As are summarized in Table I.

The positive-parity yrast band in ^{73}As determined from the present work is shown in Fig. 1 as band B1. Prior to this work, this sequence was known up to spin $J^\pi = 25/2^+$ [14]. The present study confirms the previously reported states in band B1, at excitation energies of 428, 1037, 1949, 2966, and 4083 keV, with spins $9/2^+$, $13/2^+$, $17/2^+$, $21/2^+$, and $25/2^+$, respectively. This band is extended up to spin $J^\pi = (37/2^+)$ and excitation energy ~8.6 MeV. Figure 2 is a representative γ-γ coincidence spectrum gated on the 1329-keV γ ray, showing the newly identified transitions in band B1. Three new γ transitions with energies 1329, 1497, and 1702 keV are observed in coincidence with all the low spin transitions of band B1. The measured R_{DCO} ratios (Table I) for 1329 and 1497 keV transitions obtained by gating on the 609-keV transition ($\Delta J = 2$) are consistent with $\Delta J = 2$ character, suggesting $J = 29/2^+$, $33/2^+$ spin assignments for the levels at 5412 and 6909 keV, respectively. We could not measure the DCO ratio for the 1702-keV γ ray due to low statistics. Quadrupole character is assigned for this transition. Based on the coincidence and intensity arguments, this transition is placed above $33/2^+$, which extends the band B1 up to a tentative spin $J^\pi = (37/2^+)$.

Two new positive-parity non-yrast bands labeled as group G1 are also established in the present work. These bands decay to the $J^\pi = 17/2^+$ state in band B1 through linking transitions of energy 1101 and 1541 keV. These are identified up to $J^\pi = (27/2^+)$ and $(29/2^+)$ with the addition of 974, 1388 and 1096, 1367 keV transitions, respectively. The multipolarity of these transitions is assigned based on DCO ratios of linking transitions to band B1, which suggest $\Delta J = 2$ nature for the 1541- and 1621-keV transitions and $\Delta J = 1$ nature for the 1058- and 1101-keV ones. The positive-parity assignment for these bands is tentative, and based on systematics of neighboring As isotopes [13,28]

Additionally, two negative-parity bands are identified (shown in Fig. 1 as B2 and B3). In band B2, we could confirm the previously reported negative-parity states at excitation energies 67, 929, 2040, and 2848 keV, with spins $5/2^-$, $9/2^-$, $13/2^-$, and $17/2^-$, respectively. The sequence B2 is extended up to $J^\pi = (37/2^-)$ with the addition of five new γ-ray transitions of energies 903, 1119, 1262, 1302, and 1354 keV. The measured R_{DCO} values of these transitions are consistent with $\Delta J = 2$ nature, suggesting $J^\pi = 21/2^-$, $25/2^-$, $29/2^-$, and $33/2^-$, respectively. The states in the unfavored configuration (band B3) are established at level

TABLE I. Properties of observed γ rays in ^{73}As such as transition energy (E_γ), relative intensity (I_γ), DCO ratios (R_{DCO}), multipolarity of the transition (D: Dipole/Q: Quadrupole), and spins of initial and final states: (J_i^π) and (J_f^π) are listed. The energy values are rounded off to the nearest integer. Relative intensities are calculated with respect to the 609-keV transition by normalizing its intensity to a value of 100. $\Delta J = 2$ transitions are used as gating transitions for obtaining DCO ratios. Errors are given in parentheses for I_γ, R_{DCO}.

E_γ (keV)	I_γ (Rel.)	R_{DCO}	Multipolarity	J_i^π	J_f^π
317	0.6(3)	-	-	$9/2^-$	$7/2^-$
373	1.8(4)	-	D	$17/2^-$	$15/2^-$
382	2.1(4)	-	D	$13/2^-$	$11/2^-$
434	3.3(9)	-	D	$15/2^-$	$13/2^-$
440	0.8(4)	-	(D)	$21/2^{(+)}$	$19/2^{(+)}$
468	1.2(3)	-	-	-	$11/2^+$
480	4.2(5)	0.68(14)	(D)	$11/2^-$	$9/2^-$
510	5.4(9)	-	(D)	$7/2^-$	$5/2^-$
563	2.2(4)	-	(D)	$(25/2^+)$	$23/2^{(+)}$
577	2.5(3)	-	(Q)	$7/2^-$	$3/2^-$
601	3.7(3)	-	D	$9/2^-$	$7/2^-$
609	100	-	Q	$13/2^+$	$9/2^+$
724	2.2(4)	-	-	-	$13/2^+$
729	1.8(4)	-	(D)	$11/2^-$	$9/2^-$
794	7.5(8)	0.64(11)	D	$7/2^-$	$5/2^-$
797	10.7(7)	1.02(10)	Q	$11/2^-$	$7/2^-$
808	34.3(10)	1.10(9)	Q	$17/2^-$	$13/2^-$
817	14.0(12)	1.12(16)	Q	$15/2^-$	$11/2^-$
861	10.5(9)	1.12(11)	Q	$7/2^-$	$3/2^-$
862	71.2(11)	1.01(9)	Q	$9/2^-$	$5/2^-$
862	2.6(5)	-	(Q)	$13/2^-$	$9/2^-$
865	2.1(7)	-	(D)	$11/2^+$	$9/2^+$
897	9.6(7)	1.15(15)	Q	$19/2^-$	$15/2^-$
903	20.3(9)	1.12(7)	Q	$21/2^-$	$17/2^-$
912	78.3(9)	0.98(4)	Q	$17/2^+$	$13/2^+$
974	3.1(4)	1.13(18)	Q	$23/2^{(+)}$	$19/2^{(+)}$
994	4.5(5)	0.54(21)	D	$19/2^{(-)}$	$17/2^-$
1002	6.4(9)	0.92(13)	D	$13/2^-$	$13/2^+$
1017	48.9(10)	1.05(11)	Q	$21/2^+$	$17/2^+$
1058	3.9(6)	0.71(14)	D	$23/2^{(+)}$	$21/2^+$
1085	5.9(8)	1.15(15)	Q	$23/2^-$	$19/2^-$
1096	3.6(5)	-	(Q)	$(25/2^+)$	$21/2^{(+)}$
1101	9.2(7)	0.72(13)	D	$19/2^{(+)}$	$17/2^+$
1110	41.3(13)	0.99(5)	Q	$13/2^-$	$9/2^-$
1111	4.6(7)	1.17(14)	Q	$9/2^-$	$5/2^-$
1117	26.5(12)	0.98(10)	Q	$25/2^+$	$21/2^+$
1119	8.1(9)	1.10(12)	Q	$25/2^-$	$21/2^-$
1122	1.3(4)	-	-	$(23/2^-)$	$19/2^{(-)}$
1229	4.3(4)	1.15(16)	Q	$27/2^-$	$23/2^-$
1262	7.2(7)	1.16(17)	Q	$29/2^-$	$25/2^-$
1276	0.7(5)	-	-	-	$19/2^{(-)}$
1302	4.5(6)	1.20(17)	Q	$33/2^-$	$29/2^-$
1329	9.7(6)	1.08(11)	Q	$29/2^+$	$25/2^+$
1347	1.0(5)	-	-	$(27/2^-)$	$(23/2^-)$
1354	1.5(7)	-	(Q)	$(37/2^-)$	$33/2^-$
1367	0.9(4)	-	(Q)	$(29/2^+)$	$(25/2^+)$
1388	0.9(5)	-	(Q)	$(27/2^+)$	$23/2^{(+)}$
1438	5.9(7)	1.65(19)	D	$15/2^-$	$13/2^+$
1497	4.0(6)	1.17(17)	Q	$33/2^+$	$29/2^+$

TABLE I. (*Continued.*)

E_γ (keV)	I_γ (Rel.)	R_{DCO}	Multipolarity	J_i^π	J_f^π
1541	5.8(7)	1.21(16)	Q	$21/2^{(+)}$	$17/2^+$
1621	3.6(4)	1.17(18)	Q	$25/2^{(+)}$	$21/2^+$
1702	2.9(5)	-	(Q)	$(37/2^+)$	$33/2^+$

energies 861, 1658, and 2475 keV. The spin assignment is established only for the 861-keV level with $7/2^{(-)}$ from the previous work. In the present work, this sequence B3 was extended to $J^\pi = 27/2^-$ by adding three new γ-ray transitions of energies 897, 1085, and 1229 keV, which deexcite levels at 3372, 4457, and 5685 keV, respectively. The R_{DCO} values for the 897, 1085, and 1229 keV γ rays are consistent with $\Delta J = 2$ nature, suggesting level spins $J^\pi = 19/2^-$, $23/2^-$, and $27/2^-$ respectively. The negative-parity assignments for both bands B2 and B3 are adopted from previous work [14] and systematics [11–13]. Figures 3 and 4 display representative γ-γ coincidence spectra showing transitions in the negative-parity bands B2 and B3, respectively. The coincidence gates are generated using the AND logic in RADWARE.

A sequence of five new linking γ-ray transitions with energies 729, 382, 434, 373, and 524 keV, which connect the negative-parity favored (B2) and unfavored (B3) sequences, has been identified. This sequence starts from $9/2^-$ at level energy 929 keV and connects the levels with spin $11/2^-$, $13/2^-$, $15/2^-$ $17/2^-$, and $19/2^-$, respectively. In addition, a sequence (group G2) of energies 994, 1122, and 1347 keV decaying to the $J^\pi = 17/2^-$ at 2848-keV state are found to be in coincidence with all transitions in band B2 below $J^\pi = 17/2^-$. The measured R_{DCO} for 994 keV suggests dipole nature implying $J^\pi = 19/2^{(-)}$. The multipolarity of the 1122- and 1347-keV γ rays could not be determined due to low statistics. In addition to the above negative-parity bands, a few interband γ rays with energies 440, 526, 563, and 1276 keV were also identified and placed in the level scheme.

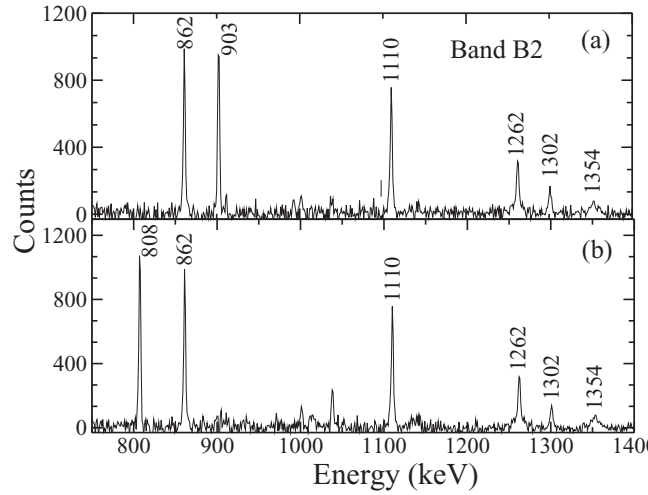

FIG. 3. Representative γ-γ coincidence spectra of ^{73}As displaying transitions in band B2, which are in coincidence with: (a) both 808- and 1119-keV γ rays, and (b) both 903- and 1119-keV γ rays.

III. DISCUSSION

In the present article, we have primarily focused on the interpretation of three main bands B1, B2, and B3. The low spin part of the one-quasiparticle positive-parity band B1 is based on the deformed proton $g_{9/2}$ orbital. These $g_{9/2}$ yrast states have been discussed earlier by several authors. Betts *et al.* [17] discussed the positive-parity states in ^{73}As below 1 MeV excitation energy, and found that these were in agreement with Coriolis interaction calculations with prolate deformation $\beta \approx 0.3$. The high-j, low-Ω intruder orbitals of the $1g_{9/2}$ shell ($1/2^+[440]$ and $3/2^+[431]$ orbitals) have a prolate shape-driving force. In particular, with regard to collective rotation, due to the strong Coriolis force, intruder orbitals (for low Ω) drive the nucleus to a prolate shape. Further, the prolate nature of the $g_{9/2}$ yrast band can be inferred from its decoupled nature (Ref. [14]). The odd proton in ^{73}As is below the $g_{9/2}$ shell and the adopted deformation is smaller than 0.3, and therefore one can expect a decoupled band built on the $g^+_{9/2}$ isomeric state.

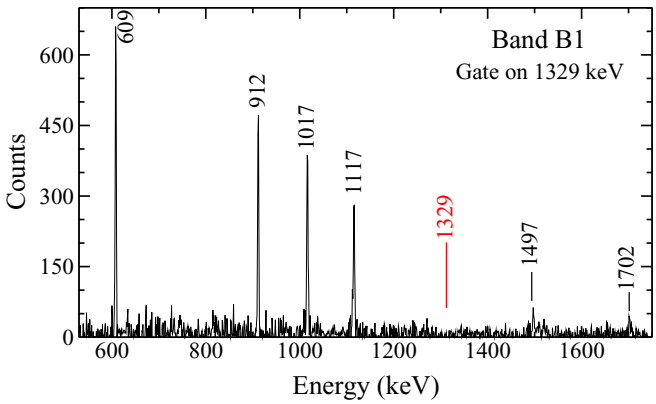

FIG. 2. (Color online) A typical γ-γ coincidence spectrum with a gate on the 1329-keV γ ray illustrating new transitions in band B1. The gating energy is indicated in red.

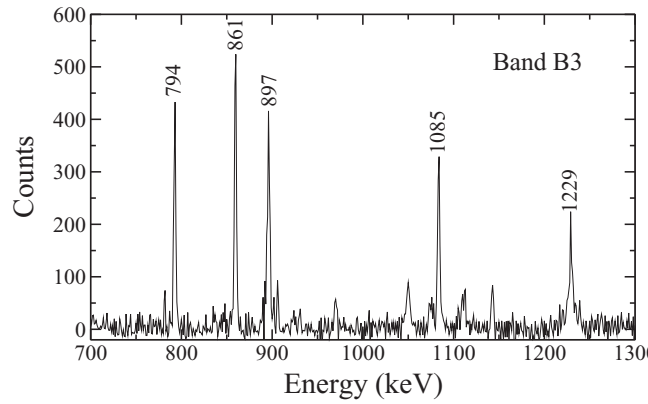

FIG. 4. A γ-γ coincidence spectrum illustrating transitions in band B3, which are in coincidence with both 797- and 817-keV γ rays.

The other aspect mentioned in Ref. [29] is that when the Fermi level is in the region of $K = 1/2,3/2$ single-particle states for prolate deformation, there is a considerable lowering of the $9/2^+$ state, and a decoupled band with the spin sequence $9/2^+$, $13/2^+$, $17/2^+$, $21/2^+$, . . . is expected. The positive-parity band B1 is one such strongly decoupled band observed in the present work confirming the predictions.

A. Cranked shell model analysis

In the present work, the positive-parity, yrast $g_{9/2}$ band B1 shows rotational character, and collectivity appears to persist up to high spin. This is evident from the kinematic moment of inertia ($J^{(1)}$) plotted as a function of rotational frequency ($\hbar\omega$), shown in Fig. 5(a). The average value of $J^{(1)}$ for the positive-parity band B1 is $\sim$20 $\hbar^2$MeV^{-1}, with a gradual increase evident around $\approx$0.5 MeV pointing to the first band crossing in band B1. This can be seen more clearly from the plot of dynamic moment of inertia ($J^{(2)}$) with respect to rotational frequency ($\hbar\omega$), shown in Fig. 5(b). The dynamic moment of inertia shows a maximum around $\hbar\omega \approx 0.5$ MeV associated with the first band crossing in band B1. For bands B2 and B3, both the kinematic and dynamic moment of inertia clearly indicate the band crossing around $\hbar\omega \approx 0.45$ MeV. Additionally, the moment of inertia for band B2 exhibits a further increase at higher rotational frequencies (beyond 0.6 MeV), possibly due to a second alignment in band B2.

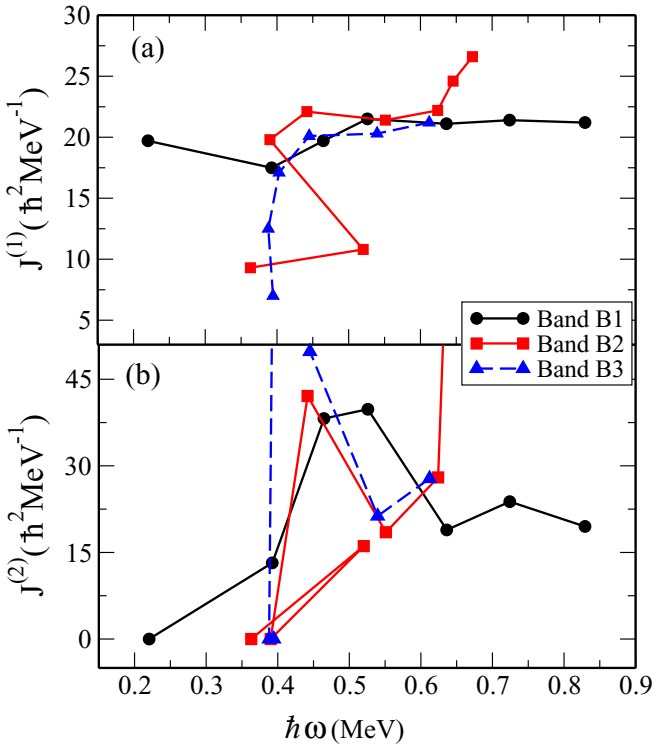

FIG. 5. (Color online) The variation of: (a) kinematic moment of inertia and (b) dynamic moment of inertia with respect to rotational frequency ($\hbar\omega$) for bands B1, B2, and B3 in ^{73}As is presented.

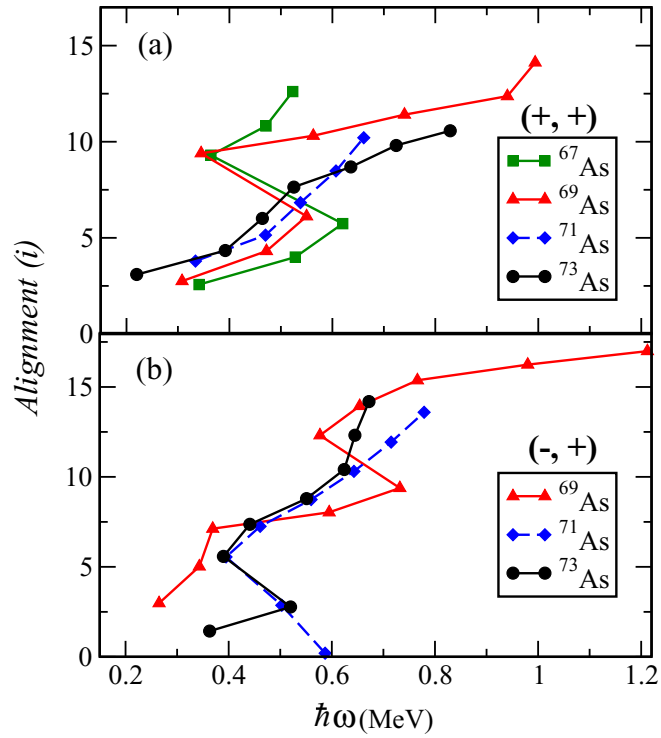

FIG. 6. (Color online) Nucleon alignments as a function of rotational frequency for the: (a) positive-parity bands and (b) negative-parity bands in odd-A As isotopes. The data for ^{73}As correspond to bands B1 and B2 in Fig. 1. Data for other As isotopes are taken from Refs. [11–13].

The alignments (i_x) as a function of rotational frequency ($\hbar\omega$) for bands B1 and B2 are compared with neighboring odd-A As isotopes in Fig. 6. The alignments for the positive-parity band B1 exhibit similar behavior as the neighboring odd-A isotope ^{71}As; the observed alignment gain at the crossing is less compared with ^{67,69}As. The positive-parity band B1 has gradual alignment around rotational frequency $\approx$0.5 MeV with moderate interaction strength between the crossing bands above the $21/2^+$ level at an excitation energy of 2966 keV. This alignment in band B1 is expected due to a pair of $g_{9/2}$ neutrons. The $g_{9/2}$ proton crossing is blocked for band B1, and in ^{73}As, is predicted at a much higher rotational frequency ($>$0.7 MeV) from our calculations. The first alignment leads to the band structure of B1 to change to a three-quasiparticle configuration: $\pi g^1_{9/2} \nu g^2_{9/2}$.

For the negative-parity band B2, the first band crossing is observed around $\hbar\omega \approx 0.45$ MeV. The alignment in this band is quite pronounced, and also has its origins in the breaking of $\nu g^2_{9/2}$ pair. Thus, the first band crossings observed in both positive- and negative-parity bands B1 and B2 are at similar rotational frequencies, and due to the proximity of the neutron Fermi surface to the $g_{9/2}$ subshell. The interaction strength is somewhat larger for the positive-parity band as compared to the negative-parity one (Fig. 7) as is evident from the quasineutron levels obtained from cranked Woods-Saxon calculations [30]. The observed alignment in the negative-parity band B2 is similar to the alignment in ^{71}As, which occurs around the same

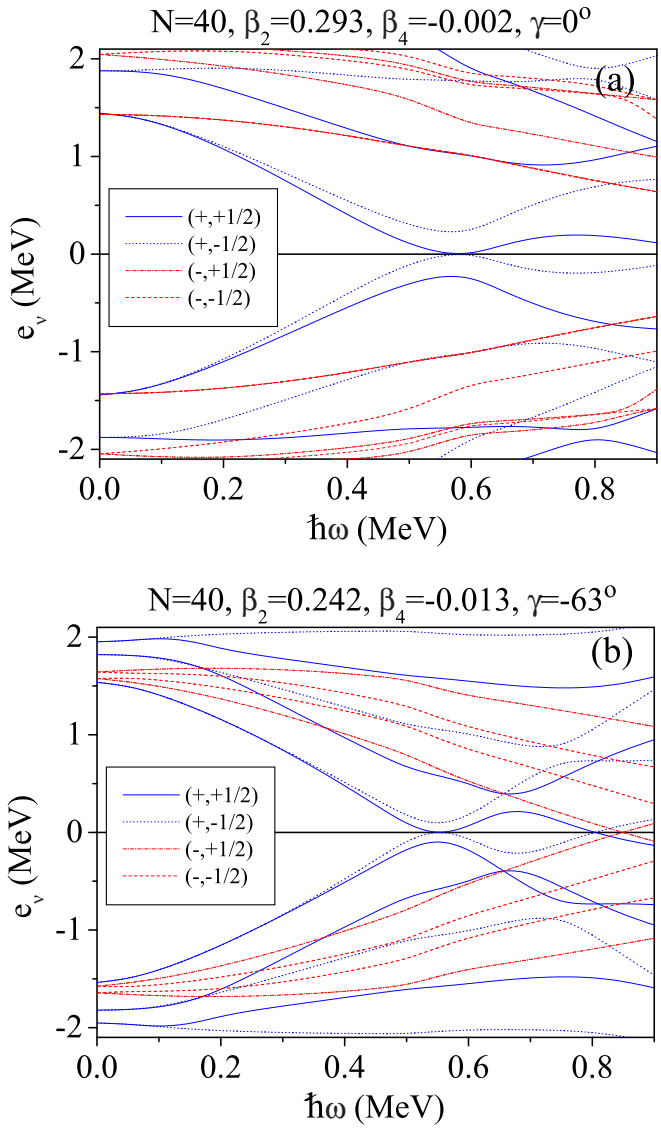

FIG. 7. (Color online) Quasineutron levels in ^{73}As for: (a) prolate deformation (b) oblate deformation, consistent with the positive- and negative-parity bands B1 and B2, respectively.

rotational frequency. This is in contrast to the first alignment in the negative-parity band of ^{69}As, which is delayed in comparison to ^{71,73}As. This may arise from differences in shapes or configurations. Further, in band B2, there is a hint of a second band crossing above $\hbar\omega \approx 0.6$ MeV. This is inferred from the up bend observed after the first band crossing in band B2 [shown in Fig. 6(b)]. This second band crossing may occur due to the alignment of a pair of $g_{9/2}$ protons, which may change band B2 into a five-quasiparticle structure above spin $25/2^-$.

B. Potential energy surfaces

We have also performed potential energy surface (PES) calculations in the β-γ plane ($0 \leqslant \gamma \leqslant 60^\circ$) based on the adiabatic constrained triaxial relativistic mean-field (RMF) calculations [31,32] with PK1 effective interaction [33]. All

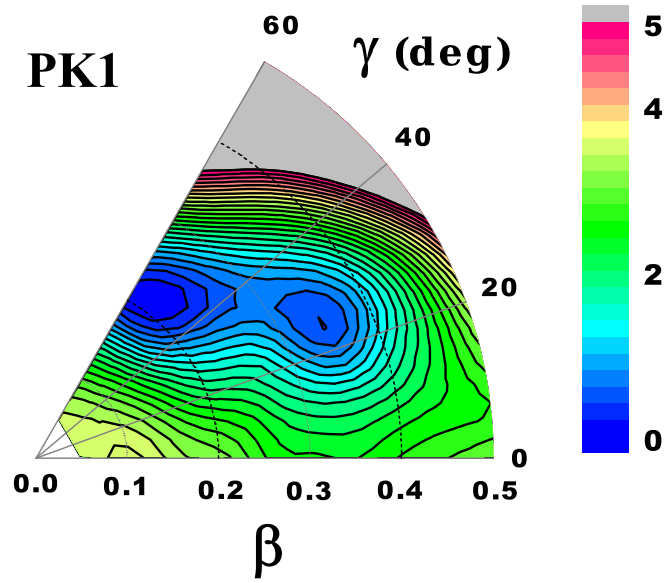

FIG. 8. (Color online) Contour plots of potential energy surface in β-γ plane ($0 \leqslant \gamma \leqslant 60^\circ$) for ^{73}As in constrained triaxial RMF calculations based on PK1 [33] effective interactions. The energy separation between adjacent contours is 0.2 MeV.

energies are normalized with respect to the binding energy of the absolute minimum, and the contours join points on the surface with the same energy (in MeV). The energy spacing between adjacent contours is 0.2 MeV. Figure 8 is a representative PES plot for ^{73}As, which clearly shows two minima, where one of the minima with $\beta = 0.20$ and $\gamma = 60^\circ$ indicates that the ground state of ^{73}As is oblate deformed, with corresponding valence proton configuration $\pi(2p_{3/2}1f_{5/2}2p_{1/2})^5$. The second minimum is located around $\beta \approx 0.35$ and $\gamma \approx 25^\circ$, and the corresponding valence proton configuration is $\pi 1g^1_{9/2}$. The energy difference between these two minima is about 0.4 MeV and corresponding barrier height is about 0.8 MeV. The energy surface around these two minima is γ soft and exhibits characteristics of shape coexistence.

C. Particle-rotor model calculations

A particle-rotor model with a quasiparticles coupled with a triaxially deformed rotor is applied to study the bands observed in ^{73}As. The model Hamiltonian of an odd-A nucleus can be expressed as

$$H = H_{\text{coll}} + H_{\text{intr}}. \tag{2}$$

Where H_{coll}, the collective Hamiltonian of a triaxial rotor, can be written as

$$H_{\text{coll}} = \sum_{i=1}^{3} \frac{\hat{R}_i^2}{2\mathcal{J}_i} = \sum_{i=1}^{3} \frac{(\hat{I}_i - \hat{j}_i)^2}{2\mathcal{J}_i}, \tag{3}$$

where $\hat{R}_i, \hat{I}_i, \hat{j}_i$ respectively, denote the angular momentum operators for the core, nucleus and the valence nucleon. The moments of inertia for irrotational flow are given by

$$\mathcal{J}_i = \frac{4}{3}\mathcal{J}_0 \sin^2\left(\gamma + \frac{2\pi}{3}i\right), \quad (i = 1,2,3), \tag{4}$$

where $\mathcal{J}_0$ depends on the quadrupole deformation β and the nuclear mass A, while γ denotes the degree of triaxiality.

$H_{\rm intr}$ in Eq. (2) is the intrinsic Hamiltonian for the valence nucleon including the Hamiltonian of the unpaired single particle H_{sp} and pairing correlation $H_{\rm pair}$,

$$H_{\rm intr} = H_{sp} + H_{\rm pair}. \quad (5)$$

The single-particle states and corresponding energies ε_ν are obtained by diagonalizing the Nilsson-type Hamiltonian H_{sp} [34,35]. The solutions of the PRM, namely, the level energies, which could be compared with the experimental data, as well as the wave functions obtained by diagonalizing the total Hamiltonian (2) in the so-called strong coupling basis. The details of the formalism and numerical methods adopted here can be found in Ref. [36]

In the PRM calculations, the quadrupole deformation parameters β are taken from the RMF calculation for the corresponding configurations of ^{73}As, while the triaxiality parameter γ is taken as a free parameter to search for the favored value. A variable moment of inertia is used, i.e., $\mathcal{J}_0(I) = \mathcal{J}_0\sqrt{1+bI(I+1)}$ [37]. The Fermi energy λ and pairing gap Δ are obtained by fixing pairing strength $G =$ 0.315 MeV. The excitation energies in the rotational spectra for both positive- and negative-parity bands are calculated using the PRM for different values of the triaxiality parameter γ, ranging from 0°–60°. Based on the results of the RMF calculations (explained in Sec. III B), the quadrupole deformation parameter $\beta \approx 0.35$ corresponding to the configuration $\pi 1g^1_{9/2}$ is adopted for the calculations of the positive-parity band and $\beta \approx 0.20$ with configuration $\pi(2p_{3/2}1f_{5/2}2p_{1/2})^5$ is employed for calculating the negative-parity states.

The calculated excitation energy spectra $E(I)$ for values of γ: 0°,20°,40°, and 60° are compared with experimental data (band B1 in Fig. 9). It is seen that for both prolate deformation ($\gamma = 0°$) and triaxial shapes ($\gamma = 20°$) calculations can well reproduce the experimental energy spectra. For both the shapes, the calculated energy spectra show large amplitude

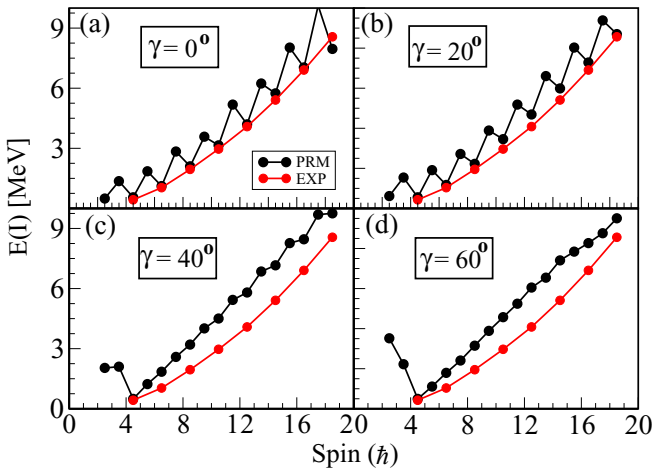

FIG. 9. (Color online) Rotational spectra for the band with positive parity calculated by PRM for different triaxiality parameter γ, and their comparison with data. The parameters $\beta = 0.35, \mathcal{J}_0 =$ 8 MeV$^{-1}\hbar^2$ and $b = 0.1$ are adopted for the calculations.

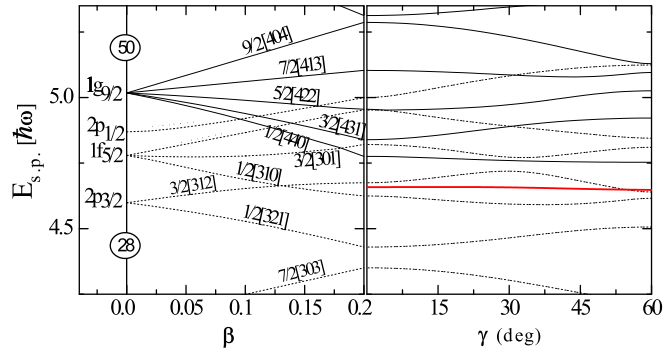

FIG. 10. (Color online) The proton single-particle energy levels calculated in Nilsson model. The red line denotes the Fermi surface.

signature splitting, thus experimentally the observation of only the favored signature partner may be understood. This is due to fact that the positive-parity band B1 has a high value of $K(=9/2)$, and therefore the valence proton, which couples to the even-even core has a weak interaction, which leads to one of the signature partner sequences being favored, while the other is unfavored. This is also reflected in the PRM calculations of the energy spectra with triaxiality γ around 0° and 20°. For near-prolate deformation, wave functions of the states in band 1 obtained by diagonalizing the single-particle Hamiltonian contain large components of the $\Omega = 1/2$ orbital from the $\pi 1g^1_{9/2}$ subshell. This could lead to the large signature splitting in this band. Whereas for the calculations with $\gamma = 40°$ and 60°, a small amplitude of signature splitting is obtained, which deviates the experimental observation. Therefore the PRM calculation suggests that triaxial deformation for the positive-parity band is more likely prolatelike deformed, fulfilled by the second minimum of the potential energy surface calculated with the RMF calculations.

The proton single-particle energy levels calculated in Nilsson model are plotted for different triaxiality parameter γ and $\beta = 0.20$ in Fig. 10, and the proton Fermi surface is found to lie between the $2p_{3/2}$ 3/2[312] and $1f_{5/2}$ 1/2[310] orbits. Rotational spectra with negative parity calculated by PRM with triaxiality parameter $\gamma = 0°,30°$, and 60° are compared with experimental data in Fig. 11. It may be seen that the rotational spectra are reasonably described for these

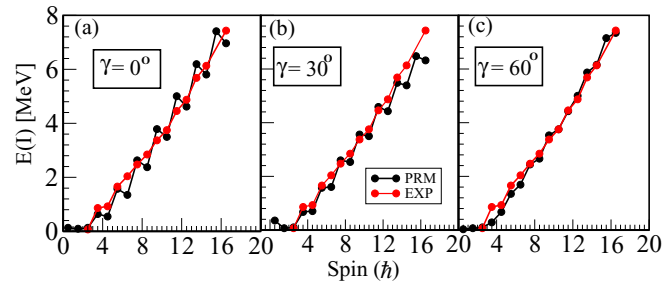

FIG. 11. (Color online) Rotational spectra for the band with negative parity calculated by PRM for different triaxiality parameter γ and their comparison with experimental data. The parameters $\beta = 0.2$ and $\mathcal{J}_0 = 8$ MeV$^{-1}\hbar^2$ and $b = 0.02$ are adopted for the calculations.

different triaxiality parameters, in particular, the calculations with $\gamma = 60^\circ$ exhibit the best agreement with experimental energy spectra. The strong mixing between single-particle components $\pi 2p_{3/2}$ and $\pi 1f_{5/2}$ has been found in this negative-parity band, as suggested in Fig. 10. Thus, the results of the triaxial particle-rotor model with adopted deformation from RMF calculations suggests triaxial-prolate-oblate shape coexistence in ^{73}As. Overall, the predictions from various theoretical approaches are found to be in qualitative agreement, and provide a satisfactory description of experimental data.

IV. SUMMARY AND CONCLUSIONS

The results of a study of high spin states in ^{73}As are presented, which were obtained through in-beam γ-ray spectroscopy using the reaction ^{64}Ni(^{12}C, $p2n$)^{73}As. The level scheme has been extended to a spin of $J = 37/2\hbar$ and an excitation energy of 8.7 MeV. A total of 30 new γ transitions were identified and placed in the level scheme. The band crossing frequencies in the positive- and negative-parity band structures are discussed in terms of CSM calculations. The observed alignment frequencies are in good agreement with the predicted ones from the single-particle Routhians calculated for both neutrons and protons.

The shape evolution in ^{73}As has been described based on RMF and PRM calculations. The experimentally observed rotational bands are compared with the triaxial particle-rotor model, and are found to be in fair agreement for specific deformation values. The calculations suggest that the positive-parity band is most likely built on the $\pi 1g_{9/2}$ configuration with a triaxial (near-prolate) shape, while the negative-parity one is characterized by the valence proton configuration $\pi(2p_{3/2}1f_{5/2}2p_{1/2})^5$ of an oblate shape. The prolate-oblate shape coexistence between positive- and negative-parity bands is also evident from the potential energy surfaces of ^{73}As obtained from the triaxial RMF calculations.

ACKNOWLEDGMENTS

We thank the Pelletron crew and other laboratories of the Inter-University Accelerator Centre for their support during the experiment. We also thank Dr. Tonev and Professor G. de Angelis from INFN, Legnaro for their support with PRM calculations. The author (M.K.R) would like to acknowledge financial support provided by UFR project fellowship (No. 42328), IUAC, New Delhi and Senior Research Fellowship (No. 09/002(0494)/2011-EMR-1) from Council of Scientific and Industrial Research (CSIR), India.

[1] J. H. Hamilton, A. V. Ramayya, W. T. Pinkston, R. M. Ronningen, G. Garcia-Bermudez, H. K. Carter, R. L. Robinson, H. J. Kim, and R. O. Sayer, Phys. Rev. Lett. **32**, 239 (1974).
[2] R. M. Ronningen, A. V. Ramayya, J. H. Hamilton, W. Lourens, J. Lange, H. K. Carter, and R. O. Sayer, Nucl. Phys. A **261**, 439 (1976).
[3] J. Döring, G. D. Johns, M. A. Riley, S. L. Tabor, Y. Sun, and J. A. Sheikh, Phys. Rev. C **57**, 2912 (1998).
[4] A. Görgen, E. Clément, W. Korten, E. Bouchez, A. Chatillon, A. Hürstel, Y. Le Coz, Ch. Theisen, J. N. Wilson, M. Zielinska, C. Andreoiu, F. Becker, P. Butler, J. M. Casandjian, W. N. Catford, T. Czosnyka, G. de France, J. Gerl, R. D. Herzberg, J. Iwanicki, D. G. Jenkins, G. D. Jones, P. J. Napiorkowski, G. Sletten, and C. Timis, Eur. Phys. J. Special Topics **150**, 117 (2007).
[5] R. B. Piercey, A. V. Ramayya, J. H. Hamilton, X. J. Sun, Z. Z. Zhao, R. L. Robinson, H. J. Kim, and John C. Wells, Phys. Rev. C **25**, 1941 (1982).
[6] A. Petrovici, K. W. Schmid, O. Radu, and Amand Faessler, J. Phys. G: Nucl. Part. Phys. **32**, 583 (2006).
[7] H. P. Hellmeister, E. Schmidt, M. Uhrmacher, R. Rascher, K. P. Lieb, and D. Pantelica, Phys. Rev. C **17**, 2113 (1978).
[8] J. Döring, G. D. Johns, R. A. Kaye, K. W. Kemper, H. Sun, G. N. Sylvan, and S. L. Tabor, Phys. Rev. C **53**, 2674 (1996).
[9] J. Heese, K. P. Lieb, L. Lühmann, S. Ulbig, B. Wörmann, D. Alber, H. Grawe, H. Haas, and B. Spellmeyer, Phys. Rev. C **36**, 2409 (1987).
[10] G. Z. Solomon, G. D. Johns, R. A. Kaye, and S. L. Tabor, Phys. Rev. C **59**, 1339 (1999).
[11] D. G. Jenkins, D. P. Balamuth, M. P. Carpenter, C. J. Lister, S. M. Fischer, R. M. Clark, A. O. Macchiavelli, P. Fallon, C. E. Svensson, N. S. Kelsall, and R. Wadsworth, Phys. Rev. C **64**, 064311 (2001).
[12] A. M. Bruce, J. Simpson, D. D. Warner, C. Baktash, C. J. Barton, M. A. Bentley, M. J. Brinkman, R. A. Cunningham, E. Dragulescu, L. Frankland, T. N. Ginter, C. J. Gross, R. C. Lemmon, B. MacDonald, C. D. OLeary, S. M. Vincent, R. Wyss, C. H. Yu, and N. V. Zamfir, Phys. Rev. C **62**, 027303 (2000).
[13] R. S. Zighelboim, S. G. Buccino, F. E. Durham, J. Döring, P. D. Cottle, J. W. Holcomb, T. D. Johnson, S. L. Tabor, and P. C. Womble, Phys. Rev. C **50**, 716 (1994).
[14] B. Heits, H.-G. Friederichs, A. Rademacher, K. O. Zell, P. von Brentano, and C. Protop, Phys. Rev. C **15**, 1742 (1977).
[15] B. O. ten Brink, P. van Nes, C. Hoetmer, and H. Verheul, Nucl. Phys. A **338**, 24 (1980).
[16] P. van der Merwe, E. Barnard, J. A. M. de Villiers, and J. G. Mallan, Nucl. Phys. A **240**, 273 (1975).
[17] R. R. Betts, D. J. Pullen, W. Scholz, and B. Rosner, Phys. Rev. Lett. **26**, 1576 (1971).
[18] R. D. Meeker and A. B. Tucker, Nucl. Phys. A **157**, 337 (1970).
[19] H. Toki, A. Faessler *et al.*, Phys. Lett. B **63**, 121 (1976).
[20] G. K. Mehta and A. P. Patro, Nucl. Instrum. Methods A **268**, 334 (1988).
[21] S. C. Pancholi and R. K. Bhowmik, Ind. J. Pure and Appl. Phys. **27**, 660 (1989).
[22] S. Muralithar, Pramana - Journal of Physics **82**, 769 (2014).
[23] B. P. Ajith Kumar, J. Kannaiyan, P. Sugathan, and R. K. Bhowmik, Nucl. Instrum. Methods A **343**, 327 (1994).
[24] B. P. Ajith Kumar, E. T. Subramaniam, K. Singh, and R. K. Bhowmik, *Proceedings of the Symposium on Advances in Nuclear and Allied Instrumentation (SANAI-97), Trombay, India*, Vol. 28 (Tata Mcgraw-Hill, New Delhi, 1997), p. 13.
[25] R. K. Bhowmik, S. Muralithar, and R. P. Singh, Proceedings of the DAE-BRNS Symp. on Nucl. Phys. B **44**, 422 (2001).
[26] D. C. Radford, Nucl. Instrum. Methods A **361**, 297 (1995).

[27] A. Krmer-Flecken, T. Morek, R. M. Lieder, W. Gast, G. Hebbinghaus, H. M. Jger, and W. Urban, Nucl. Instrum. Methods A **275**, 333 (1989).
[28] Shi-Peng Hu, Hai-Liang Ma, Xue-Peng Cao, Xiao-Guang Wu, Huan-Qiao Zhang, Hui Hua, Jun-Jie Sun, Hui-Bin Sun, Chuang-YeHe, Yun Zheng, Guang-Sheng Li, Cong-Bo Li, Shun-He Yao, Bei-Bei Yu, Jin-Long Wang, Hong-WeLi, Yi-Heng Wu, Jia-Jian Liu, Peng-Wei Luo, ChuanXu, and Yi-Yuan Cheng, Phys. Lett. B **732**, 59 (2014).
[29] C. Protop, B. Heits, H. G. Friederichs, K. O. Zell, and P. von Brentano, Z. Physik **271**, 65 (1974).
[30] W. Nazarewicz, J. Dudek, R. Bengtsson, T. Bengtsson, and I. Ragnarsson, Nucl. Phys. A **435**, 397 (1985).
[31] J. Meng, J. Peng, S. Q. Zhang, and S.-G. Zhou, Phys. Rev. C **73**, 037303 (2006).
[32] J. Meng, J. Peng, S. Q. Zhang, and P. W. Zhao, Front. Phys. **8**, 55 (2013).
[33] W. Long, J. Meng, N. Van Giai, and S.-G. Zhou, Phys. Rev. C **69**, 034319 (2004).
[34] S. E. Larsson, G. Leander, and I. Ragnarsson, Nucl. Phys. A **307**, 189 (1978).
[35] I. Ragnarsson and P. B. Semmes, Hyper. Interact. **43**, 423 (1988).
[36] B. Qi, S. Q. Zhang, S. Y. Wang, and J. Meng, Int. J. Mod. Phys. E. **18**, 109 (2009).
[37] C. S. Wu and J. Y. Zeng, Commun. Theor. Phys. **8**, 51 (1987).